Pore-Size and Shape Effects on the Recarbonation Performance of Calcium Oxide Submitted to Repeated Calcination/Recarbonation Cycles

Diego Alvarez* and J. Carlos Abanades

Instituto Nacional del Carbón (CSIC), C/Francisco Pintado Fe, No. 26, 33011 Oviedo, Spain

Received June 9, 2004. Revised Manuscript Received October 20, 2004

The use of carbonation/calcination cycles of $CaO/CaCO_3$ is emerging as a viable technique for the capture of CO_2 generated in the combustion of coals for power generation. Specifically, the choice of natural limestones as CO_2 carriers is an attractive option because they are cheap and abundant materials, although previous studies indicate that the reactivity of the calcines toward CO_2 rapidly drops with cycling. This paper reports on the effects of the internal morphology of CaO particles on their capability of absorbing CO_2. Calcines of a natural limestone with different initial textures were repeatedly submitted to carbonation/calcination conditions (up to 100 cycles). The textural evolution, as well as the carbonation conversion, of the calcined and recarbonated samples was followed along the experiments. In addition to the known mechanisms of deactivation due to grain growth and limited diffusion of CO_2 through the product layer, we have found that pore closure is also taking place in our samples, together with an overall shrinkage of the particle. All of these factors play a role in limiting the maximum carbonation conversions to around 10% after just 100 cycles.

Introduction

CO_2 capture from large stationary sources and storage in a suitable geological formation is emerging as a promising mitigation option of climate change.[1] When it is applied to gas and coal-fired power plants, there is a high economic and efficiency penalty mainly because of the capture step.[2] The separation of a pure CO_2 stream from the exhaust gases leaving a power plant, which typically contains 3−15% CO_2, is a challenging engineering task that has not yet been demonstrated at the very large scales and with the typical flue gas characteristic of power generation systems. For this "postcombustion" CO_2 capture route, various separation options are available, including close-to-commercial amine-scrubbing systems,[3] membranes,[4] and a range of adsorption/desorption[5] techniques.

Silaban and Harrison[6] and Shimizu et al.[7] proposed the use of calcium-based sorbents to capture CO_2 from gases at high temperatures based on the reversibility of the reaction

$$CaO(s) + CO_2(g) \rightleftarrows CaCO_3(s)$$

The basic carbonation/calcination loop was successfully tested[8] in the Acceptor Gasification Process in the USA during the late 1960s, in a 40 tons/day pilot plant, where the calcinations were conducted under air. For a CO_2 postcombustion capture system, the carbonation reaction makes use of CO_2 contained in the exhaust gases of the boiler, and the calcination of the formed $CaCO_3$ is carried out in a different reactor burning part of the fuel with oxygen,[7] generating a concentrated stream of CO_2 suitable for storage.

The applicability of this method requires that the reaction works fast in both directions. For the recarbonation reaction, it has been well reported[6−10] that, after a rapid, chemically controlled initial carbonation period, a much slower second stage is reached, which strongly limits the carbonation conversions. The transition between the fast and slow reaction periods was shown to take place quite suddenly at a given level of conversion, which decreases rapidly with the number of carbonation/calcination cycles.[6−12] This change of the reaction rate is attributed to the formation of a product

* E-mail: diegoalv@incar.csic.es.

(1) Banuri, T.; et al. UN Intergovernmental Panel of Climate Change, Technical Summary of the Working Group III; Report "Climate Change 2001: Mitigation", 2001.
(2) Herzog, H. What future for carbon capture and sequestration? *Environ. Sci. Technol.* **2001**, *4*, 148A−153A.
(3) Erga, O.; Juliussen, O.; Lidal, H. Carbon dioxide recovery by means of aqueous amines. *Energy Convers. Manage.* **1995**, *36* (6−9), 387−392.
(4) Feron, P. H. M.; Jansen, A. E.; Klaassen, R. Membrane technology in carbon dioxide removal. *Energy Convers. Manage.* **1992**, *33* (5−8), 421−428.
(5) Yong, Z.; Mata, V.; Rodrigues, A. E. Adsorption of carbon dioxide at high temperature−a review. *Sep. Purif. Technol.* **2002**, *26*, 195. Silaban, A.; Harrison, D. P. *Chem. Eng. Commun.* **1995**, *137*, 177−190.
(6) Silaban, A.; Harrison, D. P. High-temperature capture of carbon dioxide: characteristics of the reversible reaction between CaO(s) and CO_2(g). *Chem. Eng. Commun.* **1995**, *137*, 177.
(7) Shimizu, T.; Hirama, T.; Hosoda, H.; Kitano, K.; Inagaki, M.; Tejima, K. *Trans. Inst. Chem. Eng.* **1999**, *77A*, 62−68.
(8) Curran, G. P.; Fink, C. E.; Gorin, E. Carbon dioxide−acceptor gasification process. Studies of acceptor properties. *Adv. Chem. Ser.* **1967**, *69*, 141.
(9) Abanades, J. C.; Alvarez, D. *Energy Fuels* **2003**, *17*, 308−315.
(10) Mess, D.; Sarofim, A. F.; Longwell, J. P. *Energy Fuels* **1999**, *13*, 999−1005.
(11) Abanades, J. C. *Chem. Eng. J.* **2002**, *90* (3), 303−306.
(12) Barker, R. J. *Appl. Chem. Biotechnol.* **1973**, *23*, 733−742.

10.1021/ef049864m CCC: $30.25
Published on Web 12/15/2004

layer surrounding the CaO, which, once a certain thickness is reached, severely hampers the carbonation of the inner core.[10,12,13] On the other hand, in sorbents with a high specific surface area, the carbonation conversion is limited by the lack of void space for the growth of the product layer. Bathia and Perlmutter[13] showed that the recarbonation of the first calcine is already restricted to around 70% because of limitations in the pore volume associated with sufficiently small pores (diameter smaller than 100 nm). Bearing in mind these two effects (product layer limitations and the availability of small voids), we developed a simple correlation[9] that explained the fast drop in the carbonation capacity of sorbents tested under a wide range of conditions used by several authors (particle diameters between 0.02 and 10 mm, calcination temperatures between 750 and 1060 °C, etc.) and that was consistent with observations by scanning electron microscopy (SEM). According to this model, which qualitatively agreed with the carbonation mechanism outlined by Bhatia and Perlmutter,[13] $CaCO_3$ fills up all of the available porosity made up of small pores plus a small fraction of the large voids, limited by the thickness of the product layer that marks the onset of the slow carbonation rate. Internal sintering toward larger CaO grains (and larger voids) as the number of cycles increases and the product layer diffusivity preventing the progress of conversion in large voids were the major contributors to the decay of the capture capacity. However, there were signs that other phenomena (pore blockage and particle shrinkage) could also be taking place and could be playing a role in the overall deactivation process of a given sorbent. Furthermore, quite high relative deviations were observed between data series at low conversion (high number of cycles), although these were very scarce because most published works had largely ignored the behavior of the system at cycle numbers higher than 20. It is obvious that the information on conversions for high cycle numbers may be very relevant for a continuous capture system because it determines the average activity of the sorbent in the CO_2 absorber[11,14] or the heat requirements for regeneration. Although limestones are cheap materials, it is always desirable to operate with a low makeup flow of sorbent in the capture/regeneration loop.[15] It is therefore essential to better understand all of the mechanisms responsible for the low carbonation conversion of the materials at an extended number of cycles, which is the prime objective of this work.

Experimental Section

A Spanish high-purity limestone (La Blanca) was ground and sieved to 400−600-μm diameter, and the obtained material was used in all of the experiments. All of the experimental series comprised 100 calcination/carbonation cycles. The cyclic reactions were carried out in a small fixed-bed reactor apparatus in an atmosphere of pure CO_2. This gaseous environment was chosen in order to match the conditions required to obtain a stream of pure CO_2 at the outlet of the calciner, which is the objective of the capture system described here. In regards to the carbonation stage, the maximum conversion was not affected[9] by the excess CO_2 and therefore the same 100% was used in order to simplify the experimental setup (no gas switches between calcination and carbonation). The reactor was a 1-m-high alumina tube surrounded by a vertical furnace with two independent heating elements. A basket containing the sample was suspended along the vertical axis. The reacting gas (100% CO_2, 2 L/min STP), axially injected at the base of the tube, was forced to pass through the basket and left the furnace by the upper end of the tube. The depth of the particulate bed was limited to about 3 mm (∼5 g of parent limestone), which yielded enough sample for SEM and mercury porosimetry characterization, as well as determination of carbonation conversions by thermogravimetric analysis (TGA). Solids were allowed to react 10 min for calcination (960 °C, 100% CO_2) in the bottom part of the furnace and 5−30 min for carbonation (650 °C, 100% CO_2) in the upper part. The basket was automatically raised and lowered by means of an engine placed above the furnace. Selected samples were rapidly withdrawn from the basket while in its upper position, either before (calcined samples) or after recarbonation (carbonated samples), using a suction probe. To prevent the recarbonation of the calcined samples, which were intended for further characterization, the engine was stopped in the calcination part of the furnace after the prescribed 10 min and the gas flow was switched to air until all of the CO_2 was purged off. The basket was then raised to the carbonation position, the calcined sample was readily picked and stored in an inert atmosphere, and CO_2 was again admitted into the furnace for further cycling. The actual temperature of the sample was measured with a thermocouple placed in the center of the particulate bed.

Selected subsamples were mildly crushed, dispersed on a graphite tab, and gold-coated with a ∼20-nm-thick film for their observation under a scanning electron microscope (Zeiss DSM-942). A mercury porosimeter (Micromeritics 9500) was used for the determination of pore volumes, pore-size distributions, and true and apparent densities of selected samples. As a point of nomenclature, the term "true density" is used for simplicity in this text, referring to the density measured at maximum mercury penetration, which can be eventually different from (lower than) the true density itself, i.e., the one obtained from helium penetration. Carbonation conversions were determined by sample weight loss at 900 °C in a TGA apparatus (Setaram TAG24).

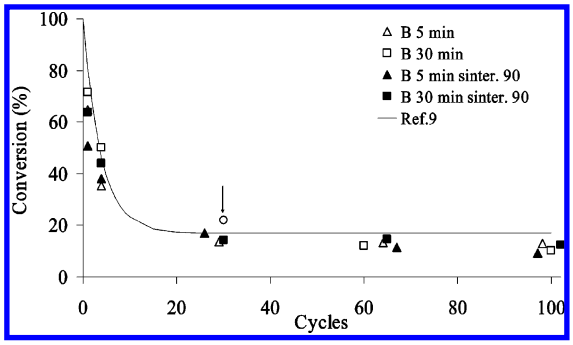

Figure 1. Conversion decay curves of the sorbents. Triangles: recarbonated 5 min. Squares: recarbonated 30 min. Void symbols: non-presintered. Filled symbols: presintered 90 min. The sample marked with a void circle is equivalent to its closest void triangle but with 30 min of recarbonation. The trend line corresponds to the correlation found in ref 9.

Results and Discussion

Figure 1 plots the carbonation conversions obtained at the end of each carbonation period in four different series of experiments (100 cycles each), using different

(13) Bathia, S. K.; Perlmutter, D. D. *AIChE J.* **1983**, *29*, 79−86.
(14) Abanades, J. C.; Anthony, E. J.; Alvarez, D.; Lu, D. Y.; Salvador, C. *AIChE J.* **2004**, *50* (7), 1614−1622.
(15) Abanades, J. C.; Rubin, E. S.; Anthony, E. J. *Ind. Eng. Chem. Res*. **2004**, *43* (13), 3462−3466.

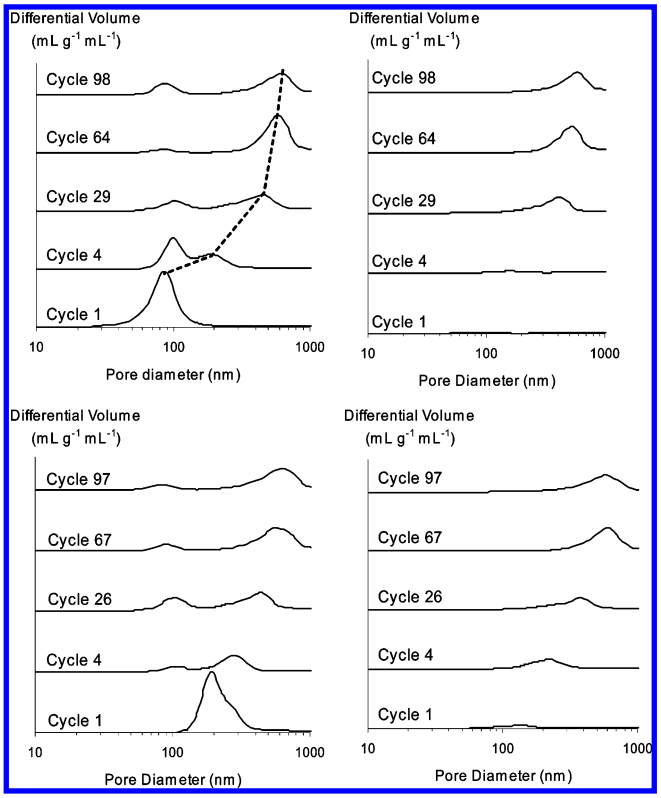

Figure 2. Intrusion curves of selected samples from the fresh CaO series (top) and the presintered series (bottom). Curves on the left correspond to calcined samples, and those on the right were obtained from their recarbonated counterparts.

times for calcination in the first cycle and different carbonation times. The series marked with filled symbols were initiated with a 90-min residence time of the sample in the calcination position (presintered samples), while the series marked with empty symbols were carried out without initial presintering. This was done, as will be discussed later, to alter the initial texture of the sorbent.[16] On the other hand, the series displayed as triangles and squares in Figure 1 correspond to carbonation times of 5 and 30 min, respectively. The differences in the carbonation performance using these different experimental conditions will be discussed later. The solid line plotted in the figure corresponds to the correlation developed in a previous work[9] and is shown here to illustrate how the behavior of the limestone used in this paper was comparable to those displayed by the variety of different limestones and experimental conditions used in that work.

Despite the overall similarity of the trends depicted by the four series of Figure 1, it can still be noticed that the conversions in the first recarbonation cycles were clearly higher (10−15%) for the fresh CaO samples (i.e., 10-min initial calcination) than for the sintered samples (90-min initial calcination). After 100 cycles, the conversion drops to very low values in all of the series, and these, in the case of the samples carbonated at 5 min/cycle, are still lower in the presintered sample (9.4%) than in the fresh CaO sample (13.1%).

The previous results could be expected from the increase in the pore size and the parallel reduction in the surface area, which must have occurred in the presintered sample. Figure 2 plots the mercury intrusion curves of selected calcined (left) and recarbonated (right) samples from the two series of experiments carried out using a 5-min carbonation time, without (top) and with (bottom) initial presintering. In this figure, it can be readily noticed that the extended residence time of CaO during the first calcination indeed provoked important changes in its pore network, with a pore-size distribution peaking at 189 nm, more than twice the size of the pores (85 nm) in the fresh CaO, calcined for 10 min. However, despite this initial difference, the behavior of both systems rapidly converges to become virtually indistinguishable from each other after the 30th cycle. This is due to the fact that calcium carbonate formed during carbonation does not keep a memory of its previous calcinations and recarbonations, in regards to its textural development. Thus, when the sintered CaO is recarbonated and then calcined (but not sintered) again, the texture development of this newly formed CaO is essentially the same as that in the fresh calcine of the nonsintered series. As the recarbonation progresses from the free surfaces inward, the unreacted CaO after completion of the first cycle will presumably be situated in the skeleton of the former CaO arrangement. When this recarbonated sample is calcined again, a network of small pores (~85 nm) is formed on the surface of the larger pores formed during the first calcination + sintering. Also the large pores will continuously increase in size with the number of cycles as a consequence of the internal sintering that takes place during calcination. This mechanism explains why the initial pore-size distribution splits into two different populations of pores: a decreasing one, always peaking at about 90 nm and attributable to the calcination of the newly formed calcium carbonate, and the other continuously shifting to bigger sizes (dashed lines in Figure 2) and due to the sintering of the unreacted CaO. This phenomenon is further illustrated in Figure 3, where the general appearance of the calcined and recarbonated samples after extended (100) cycles is shown. The outer surface of a recarbonated particle (Figure 3a) is seen as a mosaic pattern, with some large pores connecting the grain to the inner parts. The inner surfaces (Figure 3b) exposed by mildly crushing the sample show a network of very large pores of ~1-μm diameter. The surface of the calcined sample (Figure 3c) is seen as an arrangement of CaO spheres leaving between a network of very small pores. Finally, the fracture surface of Figure 3d shows the same pore network of the carbonated sample but with a grainy appearance in the surface of these pores, corresponding to the calcination of the carbonate thin product layer formed in the previous cycle.

In the scenario described so far, extended recarbonation times should not noticeably raise the final conversion achieved because the progress at this stage must be controlled by the slow diffusion of CO_2 through the product layer on the surface of the large CaO voids. In this context, it was somehow surprising to find that the pore-size distributions of the data series with extended carbonation times (30 min) peaked at remarkably lower pore diameters than their 5-min-recarbonation counterparts. This is illustrated in Figure 4, which shows how these calcines, even after 100 cycles, have a single

(16) Fuertes, A. B.; Alvarez, D.; Rubiera, F.; Pis, J. J.; Marban, G.; Palacios, J. M. *Chem. Eng. Commun.* **1991**, *109*, 73−88.

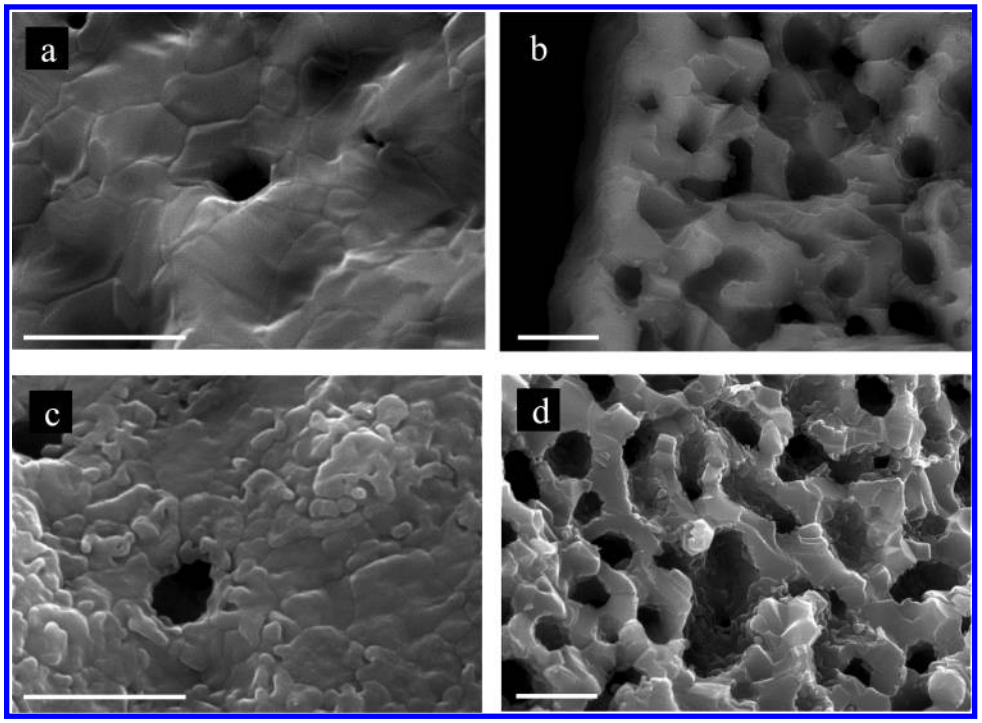

Figure 3. SEM micrographs of recarbonated (top) and calcined (bottom) samples (100 cycles, non-presintered; recarbonation time, 5 min). Images on the left correspond to free surfaces, while those on the right are fracture surfaces showing the inner arrangement of the sorbents. Scale bar: 2 μm.

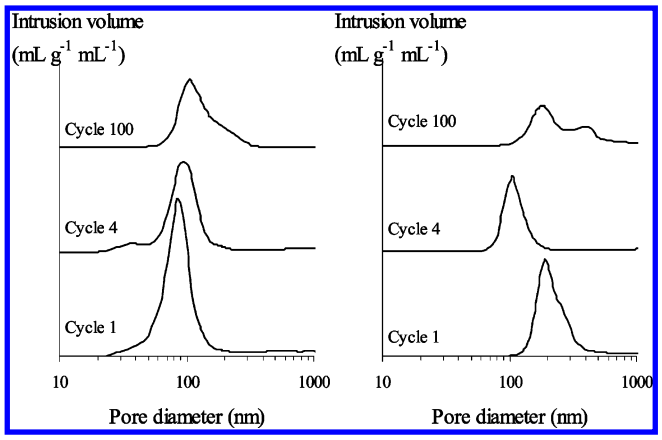

Figure 4. Intrusion curves of calcined samples (calcination, 10 min; recarbonation, 30 min). Left: no presintering. Right: presintered samples.

population of pore sizes peaking at about 80−105 nm, in the same range as the pore sizes in the fresh CaO (only slightly bigger in the case of the presintered sorbents). No bigger pore sizes were detected at all. In particular, the low conversions (10.4 and 12.4 for the fresh and presintered samples, respectively) of the calcines at 100 cycles do not match their pore-size distributions, typical of a highly reactive fresh calcine like, for instance, the same calcines after only one or four cycles, plotted just below in the same graph. On the other hand, the intrusion curves of the corresponding recarbonated samples are not shown here because they are just straight horizontal lines, indicating virtually no pore volume, and this is clear proof that these recarbonated samples have undergone extensive pore-mouth blockage. This also explains why the pores in the calcined samples were so small: when the pore-blocking carbonate is calcined, it forms a fresh CaO cap with a local pore-size distribution of around 100-nm diameter.

However, given the low conversion achieved by the sample submitted to 100 cycles, the pore volume of these small pores should be accordingly small, which is not the case. To understand this apparent contradiction, it has to be borne in mind that the mercury porosimetry technique records the volume intrusion for every given pore-mouth diameter: if a material has a large network of big pores that can only be accessed through very narrow bottlenecks, the technique will see a highly microporous material instead. Also this was indeed what happened to our calcine, as the SEM micrographs of Figure 5 demonstrate. Figure 5a is a medium-magnification image of the outer surface of a calcined particle (presintering, 90 min; recarbonation time, 30 min, 30 cycles), where it can be seen that the fine-grained surface reveals behind a regular pattern of dark spots of ~1-μm diameter corresponding to the internal pore network. The observation of this surface at a higher magnification (Figure 5b) shows the presence of smaller pores connecting the internal macropores to the outer, as hypothesized above. Finally, parts c (general view) and d (a zoom of the previous) of Figure 5 show the internal structure of the calcine (fresh fracture), where the regular pattern of ~1-μm pores can be noticed.

The extent of the pore-mouth closure in the recarbonated samples can be estimated using the mercury porosimetry data. If the true density (sample mass divided by the mercury volume displaced by the solid at 225 MPa, which penetrates all of the pores >5.5 nm) of a given recarbonated sample (ρ_r) is compared with the theoretical value (ρ_{th}) obtained through

$$\rho_{th} = \frac{1 + \frac{44X}{5600}}{\frac{1 - X/100}{\rho_c} + \frac{X}{56\rho_{CaCO_3}}} \qquad (1)$$

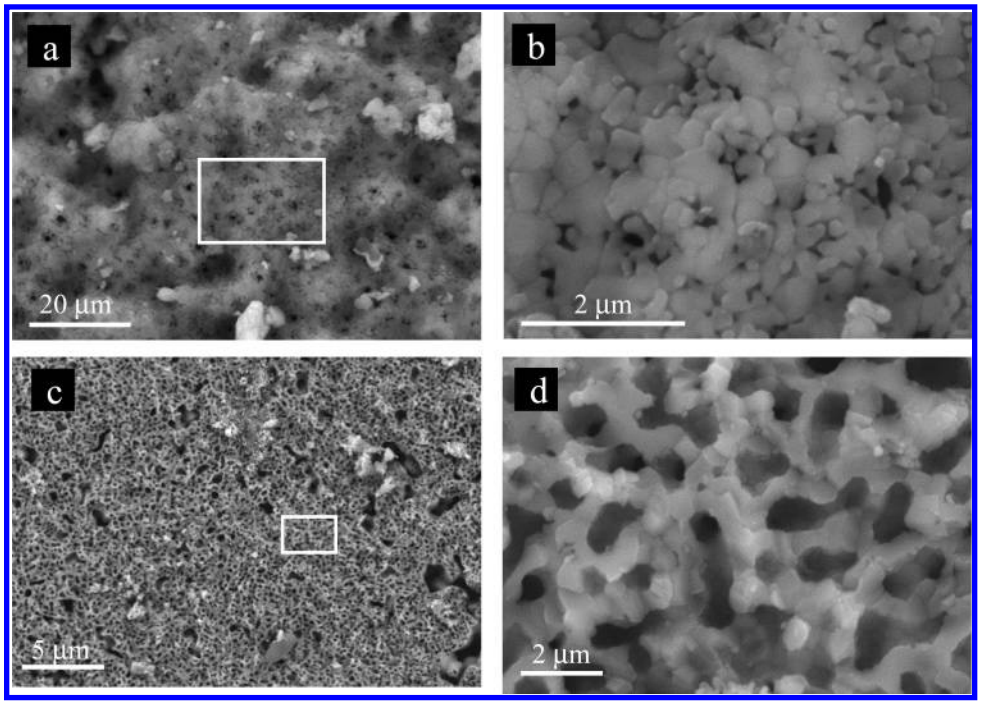

Figure 5. Appearance of a calcined sample (30 cycles, non-presintered; recarbonation time, 30 min). The dark spots in the top left image (a) indicate that a network of larger inner pores exists very close to the outer surface of the particle. Top right (b): a zoom of this image showing the typical appearance of the fresh CaO on the outer surface of the calcine. Bottom left (c): highly homogeneous appearance of fresh fracture surfaces. Bottom right (d): a zoom of the previous image illustrating the arrangement of pores of ~1-μm diameter.

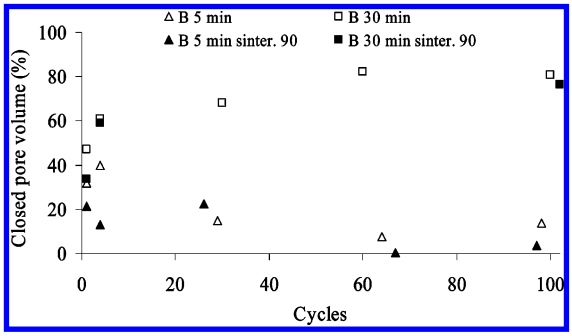

Figure 6. Percentages of occluded pore volume in the samples, relative to their total pore volume. Triangles: recarbonated 5 min. Squares: recarbonated 30 min. Empty symbols: non-presintered. Filled symbols: presintered 90 min.

where ρ_{CaCO_3} and ρ_c are the true densities of the parent carbonate (2.64 g cm^{-3}) and the calcine (variable along cycling, 3.0−3.2 g cm^{-3}) and X is the conversion expressed as a molar ratio of formed carbonate to the initial CaO. The imbalance between ρ_r and ρ_{th} can be related with the specific volume of occluded pores (V_o) using

$$V_o = \frac{1}{\rho_r} - \frac{1}{\rho_{th}} \qquad (2)$$

This was done for the samples studied here, with the result shown in Figure 6, where the percentages of occluded pore volume of the recarbonated samples (relative to the pore volume of their calcined counterparts) are plotted against the number of cycles. Again, it becomes apparent that a lot of the inner surface is being lost during recarbonation for all series with extended carbonation time, but this is not happening for shorter carbonation times. These results predict that some internal pores must have been inaccessible to the CO_2 from an early stage of carbonation, leading to an uneven distribution of the formed carbonate in the surface of the pores, and this was indeed observed in the SEM images of calcined samples given in Figure 7, which show examples of opened (left: a and c) and closed pores (right: b and d) in the fresh fractures of two highly cycled calcines. The grainy appearance of the pore surfaces on the left is evidence of carbonate loading during the previous carbonation, whereas the smooth surfaces on the right indicate that they have not sustained a carbonate layer prior to calcination.

We shall also note that, when a sample is highly cycled (30) using 5 min of carbonation time (no presintering) and then is submitted to one 30-min-long recarbonation stage, the sample has a considerably higher conversion (22%, void circle in Figure 1) and does not show appreciable signs of pore closure. This is reasonable based on the large pores present in the outer surfaces of that sorbent (Figure 3a) after 5 min of recarbonation, and it highlights the relative importance of the pore-closure mechanism that, when present, imposes a conversion of just 14% at identical number of cycles and carbonation conditions. Furthermore, this proves that the development of a thin shell in the outer surfaces of the calcined sorbent, made up of small CaO grains that leave between small pores prone to blockages during carbonation, must be a progressive phenomenon triggered by the long carbonation times in the first few carbonation cycles. In other words, the formation of narrow bottlenecks in the pore mouths of some of the calcines studied here is due to the generation of a carbonate layer in their free surfaces, which produces upon calcination a microporous cap of fresh CaO, which in turn favors the closure of the pores in the next

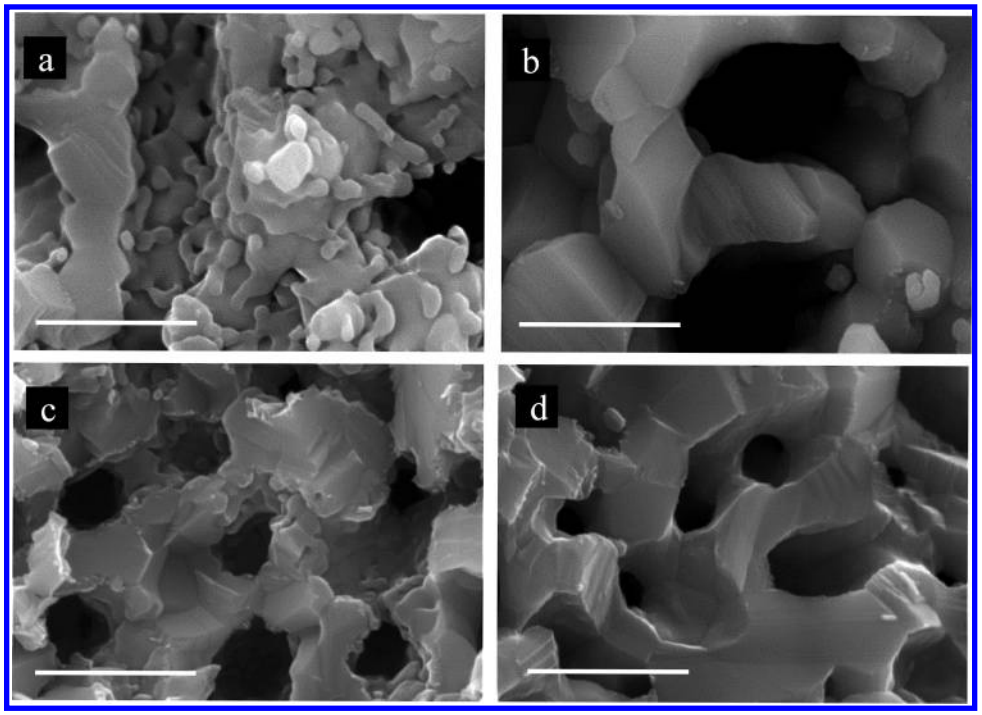

Figure 7. SEM micrographs showing two details in the fresh fracture surface of a calcined particle (presintered; recarbonation time, 30 min; 100 cycles). (A) typical grainy texture in the surface of inner pores. (B) Pores with no evidence of carbonate calcination. (C and D) Equivalent micrographs obtained from another calcine (non-presintered; recarbonation time, 5 min; 97 cycles). Scale bar: 2 μm.

carbonation, and so forth, so that the formation of a carbonate cap promotes the formation of bottlenecks and vice versa. However, a mechanism is still required to explain the enhanced reactivity of the outer surfaces compared with the bulk of the particles and the fact that no narrow pore bottlenecks were observed in the sorbents submitted to short (5 min) carbonation times. The latter can be attributed simply to the reduced carbonation time itself, which would result in lower carbonate coverage of the particle surface in the first few cycles, insufficient to promote the closure of the pore network and trigger the carbonate cap/bottleneck chain. Also the enhanced conversion of the CaO outer surfaces might be related to the increasing hindrance to the passage of CO_2 as the carbonation proceeds and/or the lack of space limitations for the growth of the product layer in the outer surfaces.

The importance of the pore blockage in limiting the maximum carbonation conversion is relative: on the one hand, it is obvious that the big drop in sorbent conversion registered with the number of cycles is not linked to this mechanism but rather to the sintering processes that take place in every calcination step. On the other hand, the residual activity of the sorbent at large cycle numbers is very relevant for a practical, continuous system, where the average particle shall have cycled the system many times. Furthermore, although it is not the subject of the present work, the pore-blockage mechanism must also be very relevant when interpreting kinetic carbonation data of highly cycled samples. Therefore, to better understand the relative importance of this pore-closure mechanism on the progress of the carbonation reaction, a more detailed study was carried out on the texture development of a single calcine during its recarbonation. This was done on the limestone submitted to 30 cycles of calcination (10 min)/recarbonation (30 min), where a pore-volume occlusion on recarbonation of about 70% had been observed in the previous experiments (Figure 6). The sample thus obtained was calcined again, and when back to the recarbonation position in the furnace, subsamples were rapidly withdrawn at selected time intervals of 0, 0.5, 1, 1.5, 2, 4, 6, 10, 15, and 30 min. To minimize the bed effects, the starting material was prepared in three runs and only four subsamples were collected in each run. The obtained partly carbonated samples were analyzed in the thermobalance in order to measure their carbonation conversions and in the mercury porosimeter for the determination of their densities and pore-size distributions. The variations of conversion and pore blockage with time are given in Figure 8. The progress of carbonation with time (Figure 8a) follows the well-known two-stage trend: a fast carbonation stage (up to about 5 min), where about 75% of the total CO_2 uptake occurs, followed by a slow, diffusion-controlled regime. In regards to the pore occlusion, it follows a similar pattern (Figure 8b): half the total pore occlusion takes place in the first 5 min, and the rest of the occlusion occurs in the next 25 min, to leave a carbonated sorbent with 62% of its porosity occluded. The shape of this curve, however, is largely conditioned by the different carbonation rates of the calcine along the experiment, as can be readily noticed in the graph of Figure 8c, where pore blockages are plotted against conversions, showing how the earlier stages of carbonation (up to 5%) take place without a substantial pore blockage, and then the pores start to continuously seal following a rough linear relationship with conversion. It now becomes obvious that a substantial part of the sorbent surface available for the reaction is being continuously lost because of pore blockages and that, even after the slow regime of carbonation is reached, pore closures are still

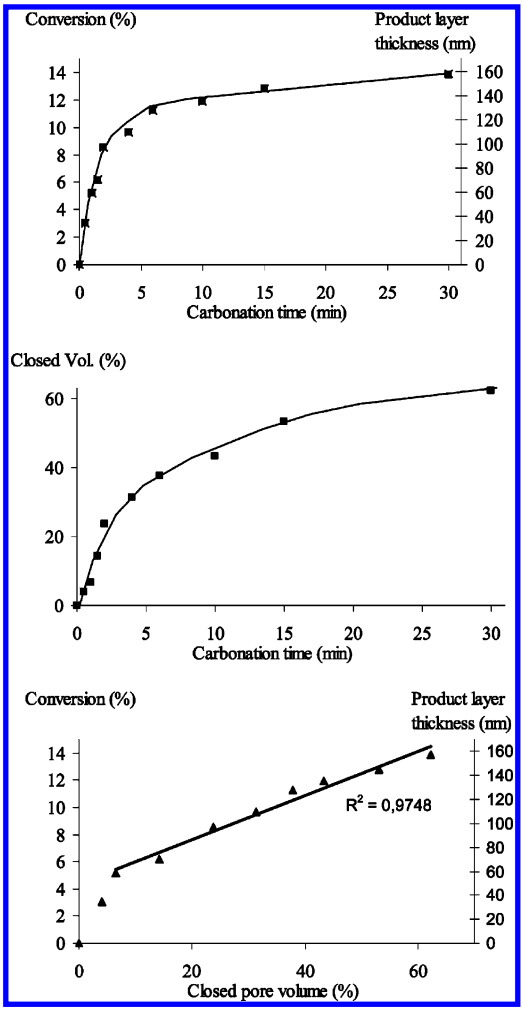

Figure 8. Structural transformations of a calcine (30 cycles; recarbonation time, 30 min; no presintering) with carbonation conversion/time. Top (a): variation of carbonation conversion and product layer thickness with time. Middle (b): variation of the percentage of occluded pore volume with carbonation time. Bottom (c): variation of conversion and product layer thickness with the percentage of pore closure.

taking place as a consequence of the marginal CO_2 uptake that occurs after 5 min of carbonation.

These samples could have evolved to substantially higher conversion if pore blockage had not been present. To quantify this loss of activity, some description of the morphology of the calcine and, in particular, of its pore network is required. As was mentioned above, the data provided by the mercury porosimetry technique are fundamentally biased because of the peculiar configuration of the pores, which can only be accessed by narrow (~100 nm) bottlenecks. An estimate is thus required of the actual pore diameters inside the calcine particles, and this can be easily obtained by SEM examination. Fortunately, the fresh fractures of these calcines look fairly homogeneous from the point of view of their pore structure, and the SEM images of Figure 5c,d are a good example of this. In these micrographs, it is clearly seen that the pore structure inside the particles can be described as an interconnected network of cylindrical pores with a diameter (D) of about 1 μm. The specific volume of this pore network (V_p) is known from the total mercury intrusion volume, which is not affected by the tortuosity of the pore entrances. Under the assumption of cylindrical pore shapes, the pore surface is calculated as

$$S = \frac{4V_P}{D} = \frac{4 \times 1.49 \times 10^{-7}\ \mathrm{m^3\ g^{-1}}}{10^{-6}\ \mathrm{m}} = 0.6\ \mathrm{m^2\ g^{-1}} \quad (3)$$

As carbonation progresses, a carbonate layer will grow on this surface. The mean thickness of this carbonate layer can be easily estimated from the above calculated specific surface area and the conversion achieved at any carbonation time. This was done for all of the partly carbonated samples (0.5−30 min) with the results shown in Figure 8a−c (right Y axis). On the other hand, if all of this surface area had been available for carbonation and assuming a final product layer thickness of 250 nm for the 30-min carbonation time (similar to previous observations[10] on CaO crystals), a conversion of 22% would have been achieved, in agreement with the value obtained from the 30-min recarbonation of the nonsealed sorbent (see Figure 1, void circle) and much higher than the 14% reported in Figure 8.

Regarding the physical effect of blockage of the product layer, it has to be borne in mind that, given the different molar volumes of CaO and $CaCO_3$ (16.9 and 36.9 cm^3/mol, respectively), about 46% of the layer thickness will penetrate into the former volume of the solid, whereas only 54% of the remaining thickness will grow at the expense of the former free pore volume. This means that, after 30 min of recarbonation, the pore radii would only be reduced by 65 nm, a rough 10%, which is too low to be noticed by the naked eye in a SEM micrograph. However, we should be able to detect this pore-size reduction in the smaller bottlenecks on the surface of the particles. Thus, if we look at the cumulative intrusion curve of the fresh calcine plotted in Figure 9, we will notice that, assuming that the product layer spreads uniformly in all of the sorbent-free surfaces, most of the internal pore volume will undergo surface closure even in the initial stages of carbonation. It has to be mentioned that the figures given here are actually very conservative because we are assuming that the product layer will be continuously growing on the surfaces of all of the pores, opened or closed, although it is likely that, once a pore is sealed, the carbonate layer will no longer increase in thickness on its surface, or it will do it only at a reduced rate, and the subsequent volume increments would be confined to the opened pores remaining at that stage, leading to more rapid layer growths and accordingly faster rates of pore closure. If this is taken into account, the thickness of the product layer in the pores opened after 6 min, for instance, would be 30% bigger than the value represented in Figure 9.

The graph of Figure 10 shows the variations of the occluded pore volume along carbonation, calculated by both density (using eq 2) and geometry considerations (Figure 9). Some discrepancies were found between the two calculations: in the first stages of carbonation, the pore closure calculated from density measurements is higher than that obtained from geometry considerations. The opposite is observed at higher conversions. However, the final pore occlusion volumes are remarkably similar from either method after a 14% conversion.

In the following paragraphs, we shall discuss, using the mercury porosimetry data, the shrinking of the

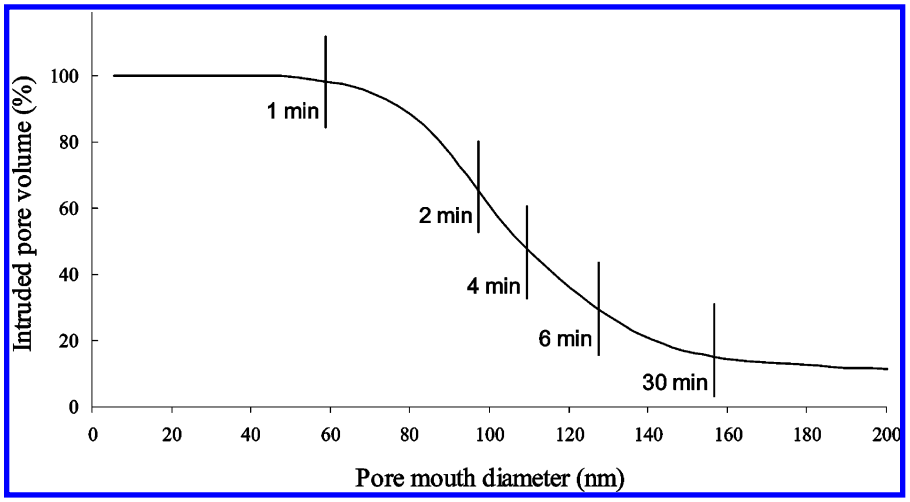

Figure 9. Cumulative intrusion curve of a calcine (30 cycles; recarbonation time, 5 min along cycling and then 30 min in the 30th cycle; no presintering), showing the thresholds for pore closure at different carbonation times.

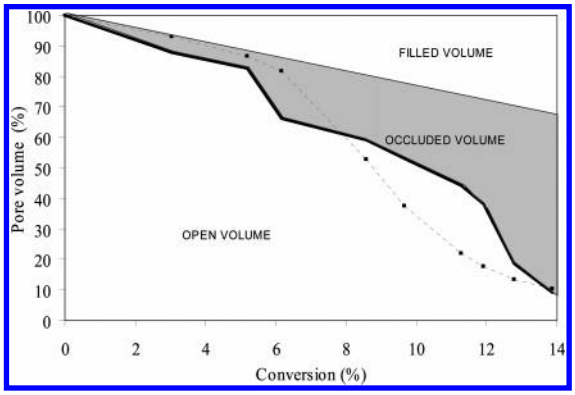

Figure 10. Apportioning of the initial pore volume of the calcine between opened, closed, and filled pores and its variation along carbonation. The solid line between open and occluded volumes was obtained from density considerations. The dashed line was calculated from the pore occlusion volumes of Figure 9.

grains during calcination and its effects on conversions. The activity of a CaO sorbent at any time along a cycling experiment, from a strictly morphological point of view, depends on its ability to accommodate the extra solid volume accumulated as a consequence of the carbonation reaction, and this is given by the porosity of CaO, which can be calculated as

$$\text{porosity}\ (\%) = \left(1 - \frac{\rho_A}{\rho_t}\right) \times 100 \qquad (4)$$

The molar volumes of CaO and $CaCO_3$ are 16.9 and 36.9 cm^3/mol, respectively,[17] and 54% porosity is theoretically left in a calcined $CaCO_3$ particle. An ideal CaO particle would therefore require true and apparent densities of 3.31 and 1.52 g/cm^3, respectively, to be able to recarbonate by 100%. The apparent (ρ_A) and true (ρ_t) densities of the selected sample used in Figures 8−10 were 2.055 and 2.964 g/cm^3, respectively, which only leaves a 30.7% porosity to accommodate the expanded product. The variation of the true density with the conversion can be calculated by eq 1, and the apparent density will similarly vary with conversion according to

$$\rho_A = \rho_{A,CaO}\left[1 + \frac{100 - 56}{56}(X/100)\right] \qquad (5)$$

and the theoretical limit for calcination will be reached when these two above values converge, that is, when the porosity is fully annihilated, and this occurs at 44% conversion in our sorbent.

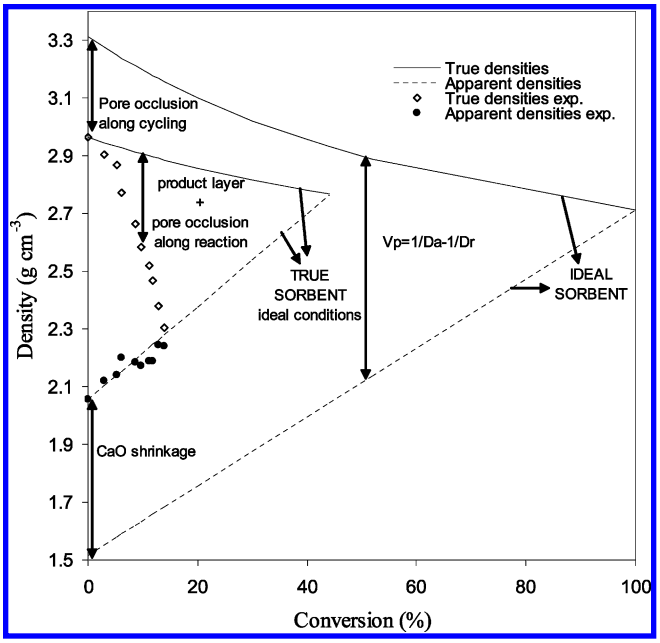

Figure 11. Evolution of textural parameters with the carbonation rate: theoretical values corresponding to the cycled sample of Figure 9 and to an ideal sorbent able to fully recarbonate. The filled and void symbols are experimental apparent and true density data, respectively.

Figure 11 plots the theoretical variations with conversion of the true and apparent densities of both the sorbent studied here and the idealized one, as well as the experimental true and apparent densities measured along recarbonation. In this figure, it can be clearly seen that our CaO departs from the ideal sorbent morphology in both the true and apparent densities. The higher apparent density of our calcine is attributed to CaO shrinkage, a well-known phenomenon of pore-volume

(17) Boynton, R. S. *Chemistry and Technology of Lime and Limestone*; John Wiley & Sons: New York, 1980.

reduction[17] and already incorporated in the overall decay mechanism of sorbent activity by sintering.[9] In regards to the reduced true density of the sorbent, compared with tabulated data[17] (3.3−3.6 g/cm^3), it cannot be attributed to a lower crystallinity of the highly cycled CaO because the literature data point precisely in the opposite direction[18] and no X-ray diffraction peak broadenings indicative of enhanced amorphousness are detected in cycled CaO or $CaCO_3$. It is, however, likely that a part of the initial particle porosity had become totally isolated from the outer in previous cycles, which would lead to an apparent reduction in the density of the solid.

The graph of Figure 11 summarizes the whole range of mechanisms responsible for the limited recarbonation of CaO particles and shows how the biggest efficiency cuts undergone by the sorbent occur during its recarbonation. Nevertheless, the figure also reveals that a substantial part of the sorbent capacity was already lost before the recarbonation reaction had even started. In view of these mechanisms, further efforts aimed at improving the capabilities of a CO_2-capture chemical loop based on limestones should focus on the following:

(i) Getting to (and maintaining along cycling) the highest surface area sorbent possible with pore diameters no smaller than, say, 150 nm. A proper selection of the sorbent might be critical.

(ii) Preventing the occlusion of pores and the shrinkage of CaO during cycling. Because these two effects are a consequence of sintering, milder calcination conditions should be sought in order to minimize them.

(iii) Avoiding the use of extended carbonation times, which might lead to the blockage of pores.

It can be concluded that the final carbonation conversion achieved by a CaO sorbent not only depends on the extent of its surface area: the geometry of this free surface also has to be able to accommodate a product layer with a maximum thickness permitted by the diffusional constraints. The process of CaO deactivation has been described in detail by other authors,[10] and it was attributed to the diffusional hindrance of CO_2 to reach the reacting surface. The explanation, although holding true for the simple geometries studied by these authors, could not be sufficient when dealing with more complex CaO arrangements such as the limestone-derived calcines used in this work, where the pore network created during calcination has to be accessed by CO_2 before carbonation can take place. It was shown how extended carbonation times can lead to the formation of narrow bottlenecks in this pore network, which could eventually limit the reaction, or at least considerably slow it down, before product layer diffusion becomes rate-limiting.

Acknowledgment. This work is partially funded by the European Commission (Grants ECSC-7220PR-125 and SES6-CT-2003-502743).

EF049864M

(18) Hyatt, E. P.; Cutler, I. B.; Wadssworth, M. E. *J. Am. Ceram. Soc.* **1958**, *41* (2), 70−74.